Journal of Geodynamics 159 (2024) 102004

Contents lists available at ScienceDirect

Journal of Geodynamics

journal homepage: www.elsevier.com/locate/jog

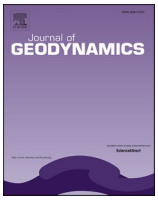

Orogen-parallel discontinuity of the Apennines subduction zone in Southern Italy as seen from mantle wedge seismic structure

Nicola Piana Agostinetti [a,b]

[a] Dipartimento di Scienze dell' Ambiente e della Terra, Universitá di Milano-Bicocca, Piazza della scienza 4, Milano, Italy
[b] Osservatorio Nazionale Terremoti, Istituto Nazionale di Geofisica e Vulcanologia, Via di Vigna Murata 605, Rome, Italy

ARTICLE INFO

Keywords:
Subduction zones
Mantle wedge structure
Apennines
Receiver function

ABSTRACT

We investigate the seismic structure of the mantle wedge of the Apennines subduction zone (Central Mediterranean) using teleseismic receiver function (RF). We inverted RF for both isotropic and anisotropic properties of the mantle wedge, from below the overriding Moho to the "plate boundary", i.e. the interface that separate the slab from the mantle wedge. Given the distribution of the seismic network, we are able to map out the change in the elastic properties at the transition between southern apennines and the Calabrian arc, given by the change in the subduction style (i.e from the subduction of continental materials to oceanic plate). We found that the anisotropy in the mantle wedge is similar between all seismic stations, generally highly anisotropic (> 10%), with a direction of the symmetry axis that rotates clockwise from North to South, following the Calabrian arc geometry and likely indicating the mantle flow driven by the slab retreat. The elastic properties of the subducted crust are more heterogeneous. To the North, the subducted crust shows a highly anisotropic (> 10%) behavior, and it occurs at larger depth (around 70 km depth), where to the South anisotropy is less intense (around 7%) and the subducted crust is shallower (around 60 km depth). These results point out a change in the subduction style that can be given by either a change in the metamorphic phase (more evolved blueschist facies stage to the North, initial greenschist facies stage to the South) or a different origin for the subducted materials (continental to the North and oceanic to the South). The differences in the anisotropic behavior of the subducted crust are reflected in the topography of the plate boundary, which becomes shallower from North to South, suggesting the existence of either a step in the slab topography or a more gentle ramp.

1. Introduction

Subduction zones are the place where most of the destructive earthquakes occur on the Earth. The "plate boundary", i.e. the surface where the two plates are in conctact each others (Abers et al., 2009; Audet et al., 2009), is able to accumulate large amount of stress, depending on many factors (like plate coupling, plunging angle of the subducted plate, physical properties of the material at the subduction interface and the presence of fluids, e.g. Schellart and Rawlinson, 2013), and release it in the so called "megathrust" events (Engdahl and Villaseñor, 2002). Geometrical properties of subduction zones, like curvature and segmentation, can also influence how and how much stress can be cumulated and released along plate boundary (Plescia and Hayes, 2020). Heterogeneity in the crustal processes can mimic complex deep lithospheric structures (Giacomuzzi et al., 2022). Thus, not considering such geometric factors can lead to un-realistic risk assessment and geodynamic modeling.

The Apennines is a segmented and highly heterogeneous subduction zone (Faccenna et al., 2001). The main geodynamic process shaping the region is the subduction of the last piece of Neotethys ocean under the European plate (Speranza et al., 2012). Such subduction has a long and complex history, starting from 90 to 80 Ma and still on-going, related to the retreat of the subduction trench toward Southeast and the opening of the oceanic basins in the Balearic and Tyrrhenian sea. During its migration, the initial geometry of the subduction zone, i.e. an almost linear trench, evolved in a more complex shape, almost triplingits width and ending up with two main arcs (Northern Apennines and Calabrian Arc). Such evolution implied the involvement of different shallow sea basins and the continental shelf, incorporating different rock materials into the subduction (Faccenna et al., 2001).

All these factors resulted in heterogeneity in the elements and processes composing the "subduction' factory" (Hacker et al., 2003) such as: (1) an heterogeneous distribution of sub-crustal earthquakes along the orogen: intermediate-depth events in Northern Apennines and

E-mail address: nicola.pianaagostinetti@unimib.it.

https://doi.org/10.1016/j.jog.2023.102004
Received 20 October 2022; Received in revised form 31 October 2023; Accepted 21 November 2023
Available online 28 November 2023

Calabrian Arc, and deep events in Calabrian arc only (Chiarabba et al., 2005); (2) the presence of windows/tears in the subducted slab mantle beneath the Southern Apennines (Lucente et al., 1999); and (3) a complex topography of the Moho across and along the Apennines orogen (Piana Agostinetti et al., 2008a,2022). Less attention has been paid to the state of the mantle wedge all along the subduction zone. Theoretical computation of the flow of the olivine in the mantle wedge during slab retreat has been widely explored (e.g. Buttles and Olson, 1988; Blackman and Kendall, 2002). However, as demonstrated by the relevance of the return-flow at slab edge (Faccenda and Capitanio, 2013), slab geometry plays a fundamental role in driving mantle flow in the wedge. This fact has been documented for the Northern Apennines (Plomerova et al., 2006; Salimbeni et al., 2007) and Calabrian Arc (Civello and Margheriti, 2004). Moreover, heterogeneity in the volatiles released from the subducted crust are known to have variously influenced the arc magmatisms along the Apennines (Cioni, 2000) and, thus, have likely modified the local elastic properties of the mantle wedge. However, due to to the limited coverage of seismic stations in the past, the details of the elastic properties of the mantle wedge along the Southern Tyrrhenian coast are still missing.

Receiver function (RF) is a passive seismic tool for investigating elastic properties and structures of the crust and upper mantle (e.g. Amato et al., 2014; Rossi et al., 2006). In particular, RF has been used to explore the anisotropic properties of the mantle wedge (e.g. Wirth and Long, 2012). Measurements of SKS splitting parameters furnish an integral contribution of the anisotropy along the ray-path (Kenyon and Wada, 2022), but they could be biased due to the presence of anisotropy in different subduction elements (see also Levin et al., 2007; Lamarque and Piana Agostinetti, 2020). Other passive seismic tools suffer from different limitations in this case: teleseismic tomography has a too low resolution at shallow ($<$ 100 km) depth (Giacomuzzi et al., 2012); local earthquake tomography can not cover adequately the mantle wedge due to the few seismic stations off-shore (Chiarabba et al., 2008; Caló et al., 2012), ambient noise suffers from strongly asymmetric source distribution and can give biased results (Fichtner et al., 2020). RF has been used many times for mantle wedge investigations (e.g. Rondenay et al., 2008; Abers et al., 2009). A preliminary study of the elastic properties of the mantle wedge in Southern Tyrrhenian sea has been done years ago (Piana Agostinetti et al., 2008b) based on the data from a single seismic station. In that study, the results highlighted the presence of a complex anisotropic stratification between the mantle wedge and the subducted crust, close to the Southern end of the Soutehrn Apennines orogen.

In this study, we extend the previous work including all seismic stations deployed along the Southern Tyrrhenian coast (nine stations), to better understand the complexity of the mantle wedge structure and its continuity across the transition between Southern Apennines and the Calabrian arc. We make use of RF analysis and RF modeling to constrain both the isotropic and anisotropic properties of the rock materials composing the mantle wedge. RF analysis is based on azimuthal stacking, which separates the "constant" component of the RF data-set, i.e. independent from the back-azimuthal direction of the P-wave arrivals, which basically gives information on isotropic behavior of the rocks, from the "periodic" component in back-azimuth (here, with a 2π-periodicity), which gives information on the anisotropic behavior of such rocks. Results, are discussed in light of the distribution of the seismic stations along the Southern Apennines and Calabrian Arc, to highlight common features and differences related to the subduction zone geometry.

2. Data and methods

We make use of teleseismic data recorded by 9 broadband seismic stations deployed along the Tyrrhenian coast, from the Southern Italy to the Calabrian Arc. Seismic stations belong to either permanent (five stations, Italian national seismic network, network code IV) or temporary (four stations, IRIS-PASSCAL experiment "CATSCAN", network code YI) seismic networks. All stations recorded data for more than 2 years, allowing us to obtain a dense back-azimuthal (baz) coverage of teleseismic sources (Fig. 1). Teleseismic events have been selected according to their epicentral distance (dist) from the seismic stations (between 30° and 100° degrees) and magnitude (larger than $M_W = 5.5$). Data-sets for permanent seismic stations obtained an almost perfect baz coverage as shown in Fig. 2. Radial (R-RF) and Transverse Receiver function (T-RF) have been computed using the frequency-domain approach developed by Di Bona (1998), which allows to robustly estimate the RF variance. The frequency-domain RF have been filtered with a Gaussian pulse of amplitude $a = 1$, which approximately indicates a frequency cut-off of 0.5 Hz. Thus, depth resolution is limited to about 3–5 km, depending on the depth range (Piana Agostinetti and Malinverno, 2018). The inverse of the RF variance is used to weight RF in the subsequent binning step. Single RF arriving from a similar baz direction and similar dist are stacked to form a "binned" RF. Bins are 10° × 20° in baz and dist, respectively, and are computed using a 50% overlapping scheme (i.e. each single RF belongs to two neighboring bins). The binning process is applied to both R-RF and T-RF datasets (Fig. 2ab). To highlight the coherence of the baz dependence of the arrivals, between R-RF and T-RF, we follow a stacking approach of the bins based on azimuthal weights (Girardin and Farra, 1998; Farra and Vinnik, 2000). This approach has been used for crustal studies (e.g. Bianchi et al., 2010a) and it is similar to standard angular harmonic RF decomposition (Bianchi et al., 2010b) that has been used to map anisotropy at crustal (e.g. Audet, 2015; Licciardi et al., 2018) and upper mantle (e.g. Shiomi and Park, 2008) depth level. The stacked bins are shown in Fig. 2c-f. The $k = 0$ stacking represents the "averaged" RF, depending only on the isotropic properties beneath the seismic station. The $k = 1$ stacking shows the 2π-periodicity in the arrivals, on both R- and T-RF, which depends either on the anisotropic properties of the rock beneath the seismic station or on the presence of dipping structures beneath the seismic station, or a combination of the two features.

To extract information about the seismic structure beneath each single station, we invert its R- and T- RF data-set using a Neighborhood Algorithm (NA, Sambridge, 1999). The NA approach is a global directed search, which is able to avoid and escape from local minima in the misfit function, for mid-to-high dimensional model-space (i.e. between 10 and 50 investigated parameters). Forward calculation, i.e. predictions of R- and T- RF dataset for a given model, are obtained using RAYSUM code (Frederiksen and Bostock, 2000). The NA algorithm and the RAYSUM code have been used together many times for RF inversion (e.g. Piana Agostinetti et al., 2017) and, in particular, RAYSUM code is well suited for investigating first-order mantle wedge structures in subduction zones (e.g. Wirth and Long, 2012). For the NA implementation, we adopt a simple mantle wedge parameterization derived from Piana Agostinetti et al. (2008b). Piana Agostinetti et al. (2008b) described in details the P-to-s phases retrieved in the RF data-set of station CUC, a seismic station at the Northern edge of the Calabrian Arc, i.e. the same P-to-s phases investigated in the present study. In Piana Agostinetti et al. (2008b), the authors tested several different parameterizations which could reproduce such P-to-s phases pattern, including the absence of anisotropy and the presence of interfaces striking in different directions, and they defined a "preferred" parameterization which reproduces all the relevant features in the CUC RF dataset. Here, we follow such preferred parameterization and we consider a six layers model: (1) a first layer for the upper crust, and (2) a second layer for the lower crust, where the interface between the two is freely orientable (i.e. could be a dipping interface); (3) an isotropic mantle lid just below the Moho; (4) a thick, anisotropic, mantle wedge layer, where the symmetry axis of the anisotropy is "positive" (following the definition in Levin and Park, 1998) and freely 3D-orientable, i.e. we are not only considering a simple horizontal axis as in SKS splitting analysis; (5) an anisotropic dipping layer representing the subducted crust (here anisotropy can be either "positive" or "negative"); and (6) the isotropic slab. The crust along the Tyrrhenian coast is generally considered thinner than the average

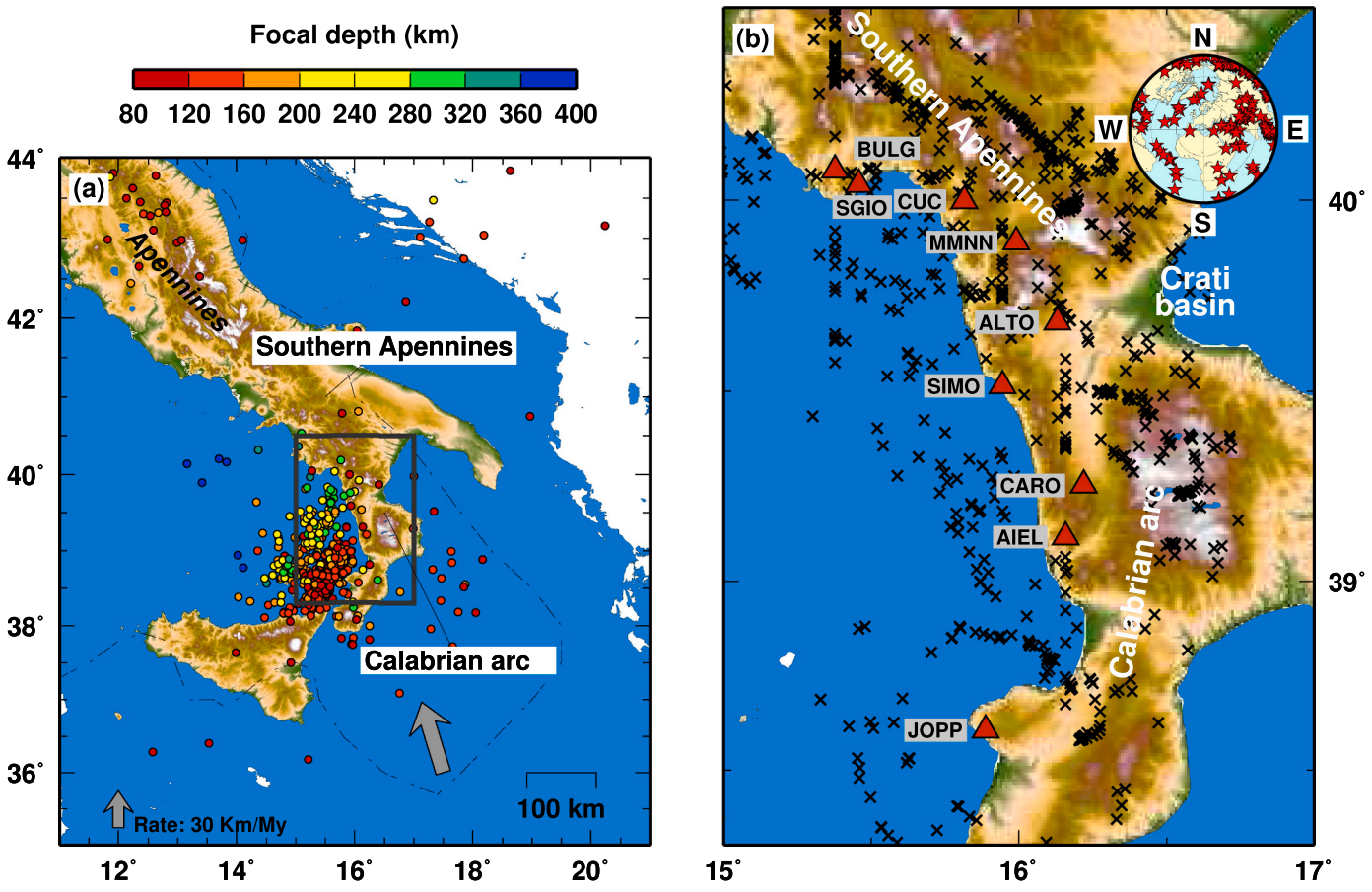

Fig. 1. (a) Topographic map of Southern Italy. The subduction trench is indicated with a dot-and-dashed line. Colored circles indicate seismic events related to subduction processes (i.e. with a focal depth larger than 80 km). The gray arrow shows the convergence direction between Africa and Europa plates in the area. Arrow length is proportional to convergence rate. The black box indicates the study area. (b) Map of the seismic network analyzed in this study. Red triangles and names indicate the seismic stations. Crosses show the teleseismic-ray piercing points at 80 km depth, for the analyzed data. The inset displays the distribution of teleseismic event analyzed for the data-set of BULG seismic station.

continental crust (e.g. Di Bona et al., 2008). It is worth noticing that, for modeling the dipping subducted crust, both top and bottom interface are dipping, forced to have the same strike and dip angles. We assume that the "preferred" parameterization, which has been originally defined for station CUC, can be adopted for all seismic stations deployed along the Calabrian Arc. While local differences in the Calabrian subduction zone are likely from North to South, also reported by geophysical observations like the distribtution of intermediate-depth seismicity, we consider the same parameterization for all seismic stations to facilitate the comparison of the results obtained for different stations. In our parametrization, the "plate boundary" (also called "subduction interface" or "slab surface", Heuret et al., 2011; McCrory et al., 2012), is represented by the interface between the two anisotropic layers, and it is freely orientable in space.

The P-to-s phases pattern shown in Fig. 2 is consistent with a third Layer ("isotropic mantle lid") that does not contain anisotropic materials, in agreement with studies on Pn phases beneath Italy which show limited anisotropy in the Southern Tyrrhenian Sea (e.g. Díaz et al., 2012). The absence of anisotropy in the lithopheric lid is likely a local feature, related to the geodynamics of the Calabrian subduction zone. The anisotropy in the fourth Layer ("anisotropic mantle wedge") displays a "positive" behavior, which is consistent with a mantle wedge composed of dry A-type olivine. As specified in Piana Agostinetti et al. (2008b), the "polarity" of the anisotropy in the subducted crust (i.e. either "positive" or "negative" as defined in Levin and Park, 1998) are poorly distinguished from R- and T-RF data-set periodicity (see examples in: Sherrington et al., 2004; Bianchi et al., 2008; Piana Agostinetti et al., 2008b), while the overall azimuthal direction and magnitude are well resolved. Thus, here, we will consider in the discussion only the azimuthal direction of the symmetry axis and the magnitude of the anisotropic behavior of the rock, in terms of percent above/below the average rock seismic velocity along the symmetry axis direction.

To summarize, the 27 free investigated parameters are: thickness of the upper and lower crust, mantle lid, mantle wedge, subducted crust (5 parameters); S-wave (V_S) velocity of the upper and lower crust, mantle lid, mantle wedge, subducted crust and slab (6 parameters); V_P/V_S ratio of the upper and lower crust, mantle lid, mantle wedge, subducted crust and slab (6 parameters); anisotropic magnitude (the same for both P-wave and S-wave) for the mantle wedge and subducted crust (2 parameters); 3D orientation of the symmetry axis in anisotropic layers, i.e. azimuth and plunge angles, for the mantle wedge and subducted crust (4 parameters); dip and strike angles for the upper-to-lower crust interface (2 parameters); and dip and strike angles for the upper and lower interfaces of the subducted crust (2 parameters).

To retrieve a robust model for each seismic station (i.e. a best-fit model), we set the NA algorithm to explore $N_s = 3$ Voronoi cell per iteration, sampling each cell with $N_r = 12$ new models. In each iteration, we keep the $N_s = 3$ best-fit models and we resample their Voronoi cells. We iterate the process for $N_{iter} = 1000$ iterations, for a total of 36,900 visited models per station (i.e. we start from 900 Voronoi cells randomly distributed in the model space). The CPU-time per station is about 15 h using 18 CPUs (about 50 min per CPU), where the 18 CPUs execute MPI directives used to sample Voronoi cells in parallel (each cell is sampled independently from the others, and each sample within a Voronoi cell

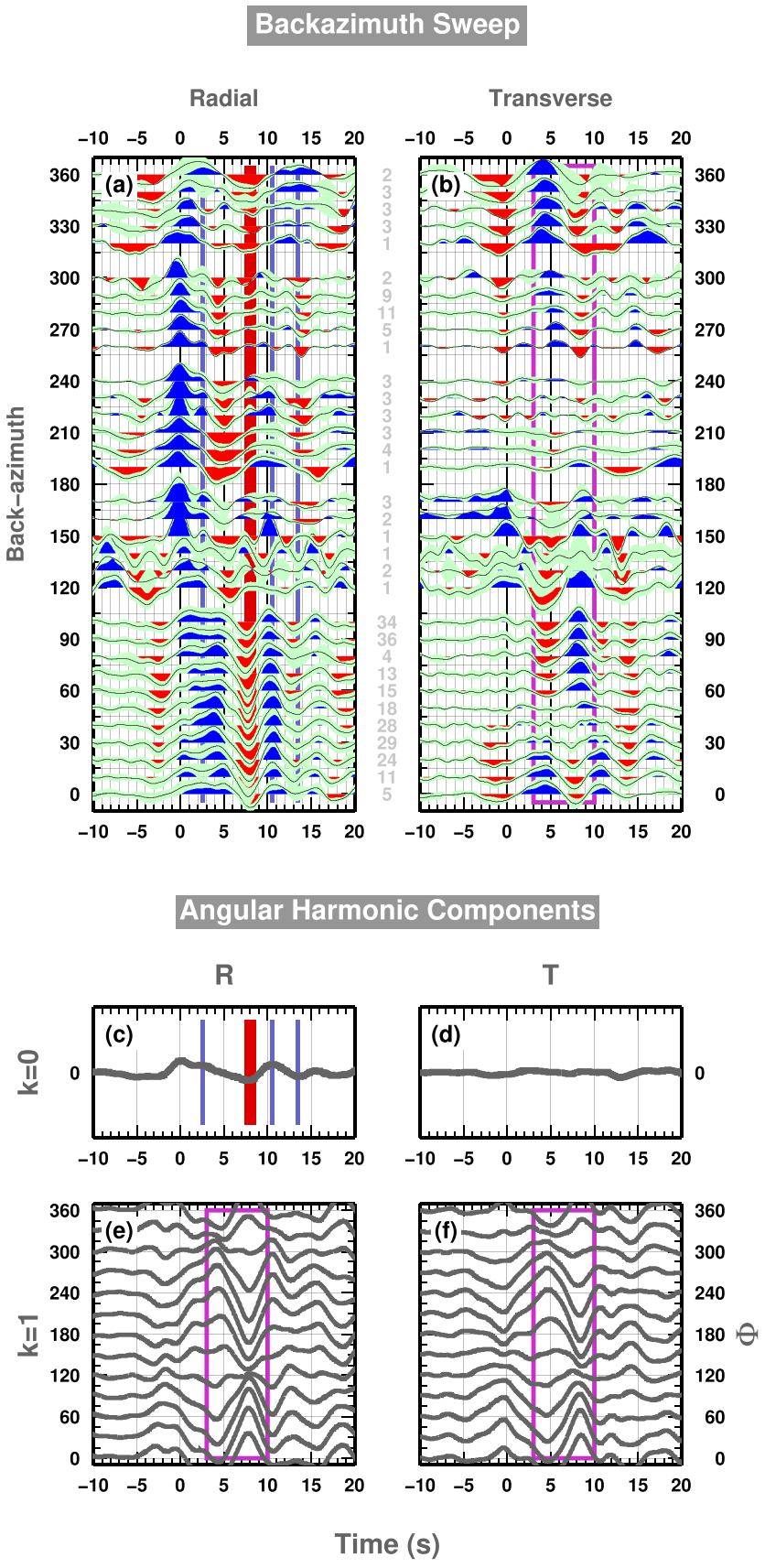

(caption on next page)

Fig. 2. Example of RF data-set (CUC seismic station). (a) Radial RF as a function of the back-azimuth (baz) of the incoming P-wave. Blue (red) wiggles display positive (negative) amplitude arrivals. Light-green area around wiggles indicates the uncertainty on the RF, computed from the binning process. Blue vertical lines show the main arrivals (Ps and multiples) from the shallow Moho discontinuity. A red vertical bar indicates a persistent (over all baz directions) negative arrival, probably related to a sub Moho low velocity region. (b) Transverse RF as a function of the back-azimuth (baz) of the incoming P-wave. Same color code as in (a). The violet box indicates the time-window where most relevant arrivals show 2π-periodic, with baz, amplitude variations. (c) First angular harmonics (k = 0) for the Radial RF. Most relevant arrivals indicated in (a) are also indicated here. (d) First angular harmonics for Transverse RF. (d) Second angular harmonics (k = 1) for Radial RF. Most coherent arrivals are visible in the violet box, same as in (b). (e) Second angular harmonics (k = 1) for Transverse RF. Same arrivals as in (d) are shown in the violet box.

can be created independently). At the end, we search for the best fit model for each station. The goodness of the model is proven from the overall fit. Low quality data-sets display a poor fit on the k = 1 stacking due to the presence of un-modellable signals (in terms of anisotropic layers or dipping interfaces, the "Unmodelled" component in Park and Levin, 2016).

3. Results

In general, the seismic data collected here seem to be adequate to the scope of the study, i.e. retrieving information about the mantle wedge seismic structure and its variations along the subduction zone. In fact, the location of the seismic stations along the Tyrrhenian coast makes the teleseismic rays, which travel with very low incidence angle at the receiver side location (i.e. almost vertically) to sample directly the mantle wedge (Fig. 1b), allowing to have a clear and almost continuous picture its structure from the southernmost tip of the Southern Apennines orogen to the Calabrian arc. Moreover, teleseismic data analyzed show a good baz coverage for almost all seismic stations, which is needed to compute robustly the baz dependence of the arrivals on both R- and T- RF data-sets (inset in Fig. 1), and, thus, to extract information about both isotropic and anisotropic properties of the rocks composing the mantle wedge.

In Fig. 2, we present an example of the RF data computed here, for station CUC. Such seismic station has been previously analyzed in a preliminary study (Piana Agostinetti et al., 2008b). The new data-sets displays an almost complete baz coverage, removing the potential ambiguities present in the previous analysis. The binned R-RF dataset displays positive arrivals at 2 s and 11 s, related to the shallow Tyrrhenian Moho (Di Bona et al., 2008). A generally-negative arrival is seen at about 8–9 s, which presents strong amplitude variations with baz (Fig. 2a). The same baz-dependence is found on T-RF data-set, for the arrival between

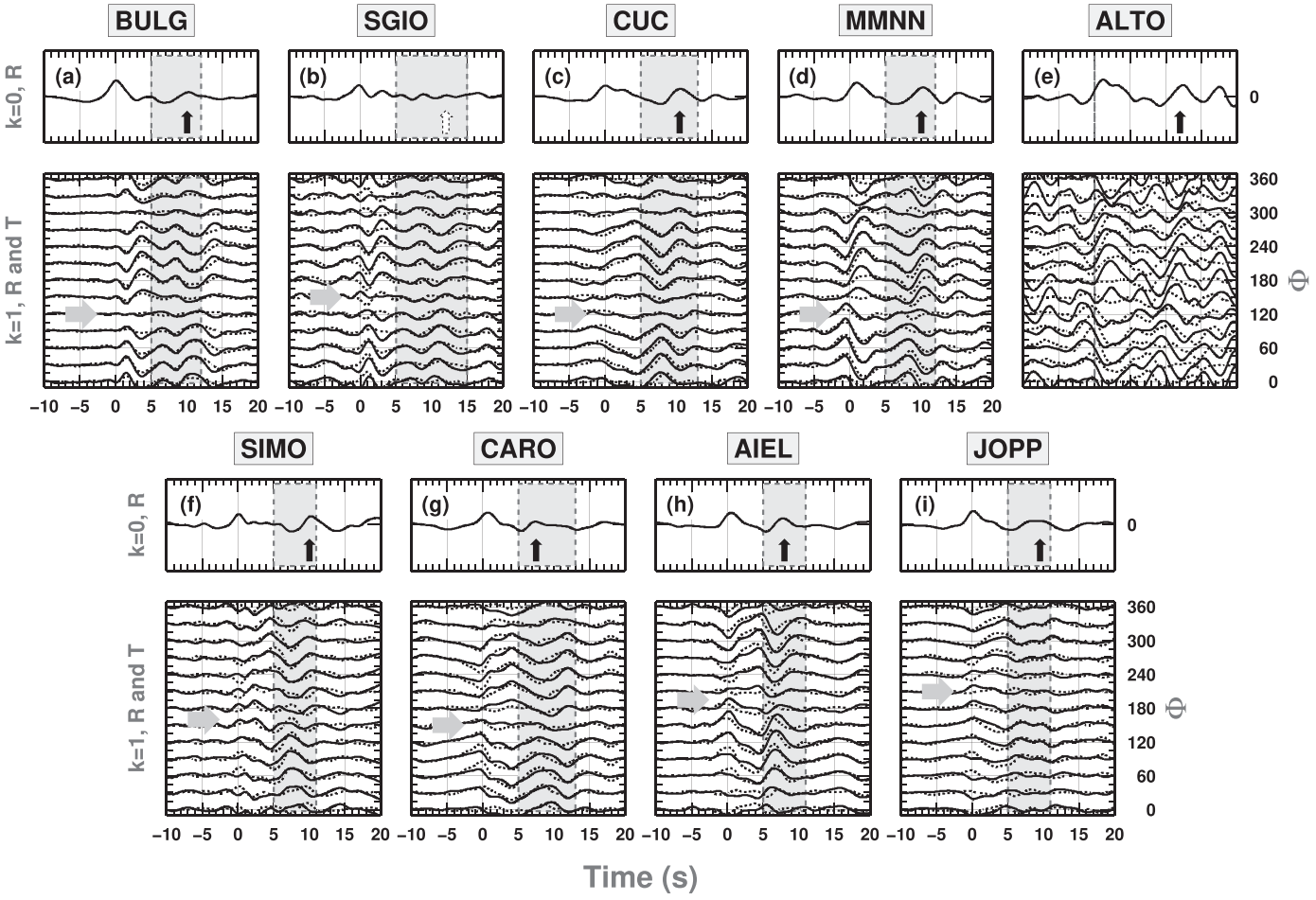

Fig. 3. Angular harmonics for all the seismic stations analyzed. For each station, the top panel shows the k = 0 harmonics for the Radial RF. The gray box indicates the time-window where most relevant periodic arrivals occurs on the k = 1 harmonics. The black arrow displays the arrival time of the most relevant positive S-wave velocity jump below the Moho. Bottom panel shows the k = 1 harmonics for the radial (black solid lines) and transverse (black dashed lines) RF. The time-window where we found a robust coherence of the k = 1 harmonics in R and T RF is indicated with a gray box. The gray arrow displays the azimuthal direction where the main periodic pulses change their polarity (i.e. the direction of the main symmetry axis of the system).

5 s and 9 s, with a polarity flip at about 45–60° baz direction (pink box in Fig. 2b). The stacking process highlights both "constant" and "variable" arrivals in the two RF data-sets. For the R-RF data-set, the k = 0 stacking displays the same features mentioned above, i.e. two positive pulses at 2 s and 11 s, and a negative one at 8 s (Fig. 2c). It is worth noticing that the negative pulse is much more clear now, when periodicity is removed. The k = 0 stacking for the T-RF data-set is almost zero, as it should be, testifying the goodness of the baz coverage. Finally, the k = 1 stacking displays exactly the same patterns in the two data-sets (pink box in Fig. 2ef), which is a clear sign of the presence of anisotropic materials at depth, as originally stated in Farra and Vinnik (2000).

In Fig. 3, we present the k = 0 stacking for the R-RF dataset (top panel), and the k = 1 stacking for both the R- and T- RF datasets (bottom panel), for all investigated stations. Stations are roughly ordered from North to South along the Tyrrhenian coast. There are some general patterns that are represented in all data-sets, and some peculiar patterns for groups of stations. First of all, we observe a great coherence in the k = 1 stacking between R-RF data-set (black lines in the bottom panel) and the T-RF dataset (dashed line in the bottom panel), especially in the gray-shaded box highlighted in both top and bottom panels. Station ALTO is the only one where un-coherent arrivals are found in the two k = 1 stacking, testifying the poor back-azimuthal coverage for this temporary station. Second, for all station but ALTO, the pulses in the gray-shaded box of the k = 1 stacking have a symmetry axis (indicated with an horizontal light-gray arrow in the bottom panel) at different baz directions, where the baz direction increases from North to South. Speaking of more local observations, the stations to the North (SGIO/BULG/CUC/MMNN/SIMO) display a positive pulse in the k = 0 stacking within the gray-shaded area, arriving always to the end of such time-window (black vertical arrow in the top panel). This pulse is missing or unclear for station SGIO. In the datasets for the southernmost stations (CARO/AIEL/JOPP), the same positive pulse arrives always at the beginning of such time-window (vertical black arrow in the top panel). All these observations point out a general complex seismic structure for the mantle wedge, where anisotropic materials and/or dipping structures must be present at a sub-Moho depth level, and they justify the parameterization presented in the previous section.

We invert the R-RF and T-RF data-sets, with a similar parameterization but independently for each seismic station, following the NA approach presented above. The NA search ends up with a family of models that fit the observation quite well, as shown in Fig. 4. As expected, the selected parameterization works for all station but ALTO,

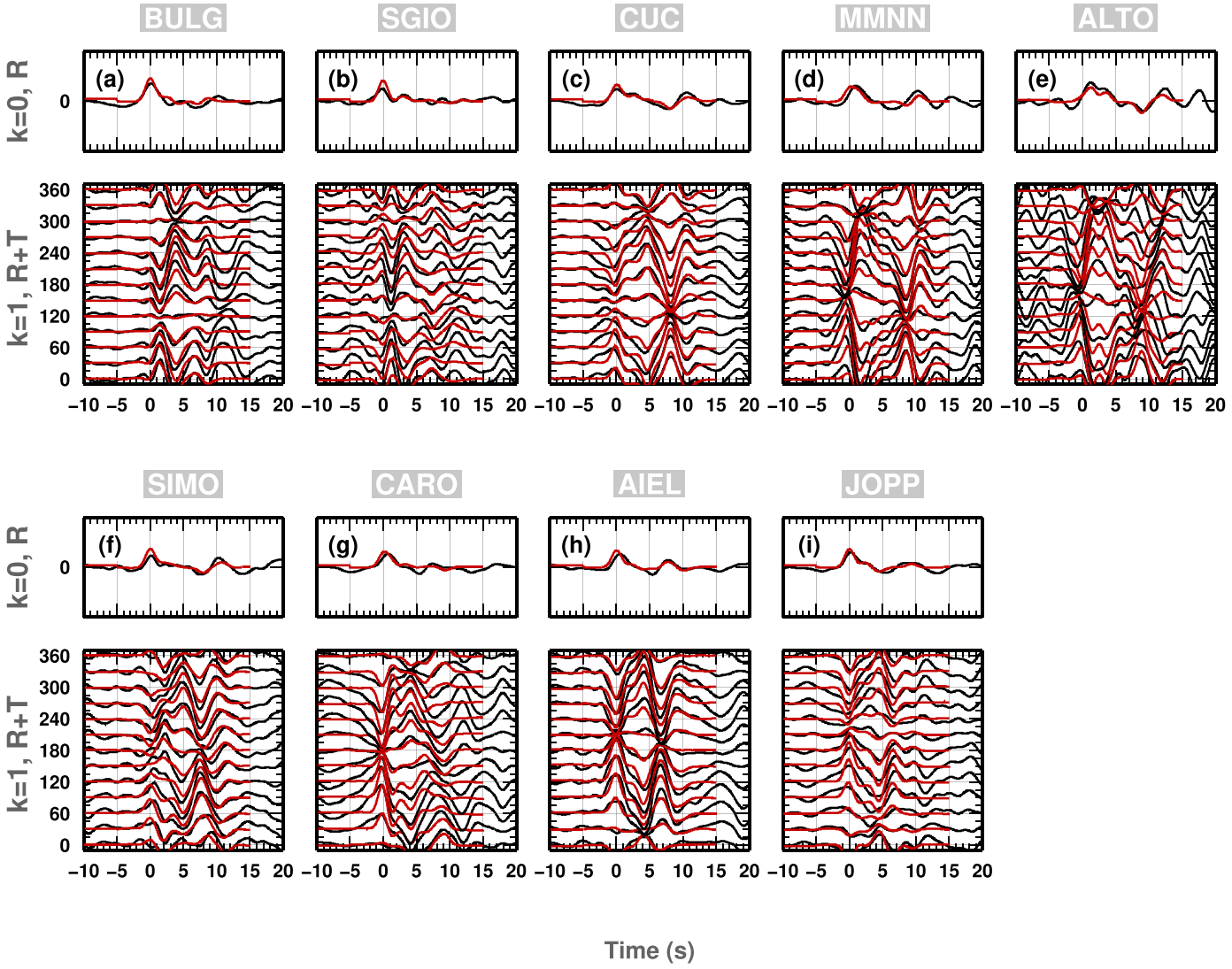

Fig. 4. Fit between observed and predicted angular harmonics, for all the seismic stations analyzed. In each panel, red lines represent the angular harmonics computed using the best-fit model for the indicated station, obtained with the neighborhood algorithm. Top panels as in Fig. 3. In bottom panel, we plotted the sum of the k = 1 harmonics for R and T RF (i.e. the sum of the solid and dashed lines in bottom panels of Fig. 3. The sum of the two k = 1 harmonics is used to highlight coherent patterns in R and T RF periodicity.

which has a strong component of "Un-modeled" (Park and Levin, 2016) contribution to the stacking. The resulting best-fit models are presented in Figs. 5 and 6. Looking to the 1D V_S profiles, we note that for all stations the anisotropy in the mantle wedge (orange boxes in Fig. 5) has a large magnitude (about 15%), without any distinction between stations to the North in the foothills of the Southern Apennines (stations: BULG, SGIO, CUC, MMNN and SIMO) or along the Calabrian arc (stations: CARO, AIEL, JOPP). On the other hand, such portion of the model is definitely thicker to the North (ranging 40–50 km think) with respect to the South (between 20 and 35 km thick). As a consequence, the "subduction interface" (i.e. the contact between the two plates, here the top of the subducted crust, which translates in our model, to the interface between the two anisotropic layers, between the two colored boxes in Fig. 5) is relatively shallower in the South with respect to the North. Two striking differences between North and South are: (1) the magnitude of the anisotropy in the subducted crust, which is much higher to the North with respect to the South; and (2) the presence of a strong "positive" (i.e. seismic velocity increases with depth) velocity jump at the bottom of the subducted crust, which is almost absent to the South.

In Fig. 6, we report a map of the the azimuthal directions of the two anisotropic layers considered in our parameterization, together with some related parameters (e.g. plate interface strike). The upper anisotropic layer (i.e. the mantle wedge in our parameterization) displays an azimuthal direction which seems coherent with the local slab curvature (i.e. it is normal to the local curvature), rotating from NE-SW, in the North, to SE-NW, in the South. The rotation seems quite continuous along the arc. All anisotropic layers show similar magnitude of anisotropy (about 10–15%). Conversely, the lower anisotropic layer (i.e. the subducted crust in our parameterization) displays quite scattered direction of anisotropy both in the South and in the North. However, as previously highlighted, the magnitude of the anisotropy for this layer is definitely larger to the North (10–14%) with respect to the South (3–8%). Finally the local strike of the plate boundary seems to be coherent with the Calabrian arc geometry, rotating from NW-SE in the North, to SW-NE to the South. The depth of the plate interface is shallower to the South (54-to-68 km depth) with respect to the North (71-to-87 km depth).

4. Discussion

Our results shed light on the elastic properties of the mantle wedge along the Southern Tyrrhenian sea, at the transition between Southern Apennines and the Calabrian Arc. All the seismic stations, exclusive of ALTO, recorded a relevant number of teleseismic events coming from different baz directions, enabling to constrain both isotropic and anisotropic properties of the rocks composing the upper mantle and subducted crust. The retrieved 1D V_S profiles for all stations display both common features and some spatial patterns, which indicate that the bulk of the mantle wedge is quite homogeneous across the transition, while the subducted crust shows more variability between stations in the North, close to the tip of the Southern Apennines, and stations directly on top of the Ionian subducted plate to the South.

In the mantle wedge, our first shallower anisotropic layer, anisotropy seems to be quite homogeneous, with a strong amplitude (about 12–15%) and a symmetry direction that rotates clockwise from North to South, coherently with the subduction trench. Such high degree of anisotropy has been already found beneath station CUC in Piana Agostinetti et al. (2008b) and it is explained as a mantle wedge shear zone above the subducted oceanic crust. Anisotropy in the mantle wedge as large as 5% is usually indicated by SKS splitting measurements. However, RF studies focused on the mantle wedge found larger values (e.g. 8–10%, Nikulin et al., 2009; Wirth and Long, 2012). Its continuity and homogeneity toward the South indicate that the process shaping the mantle wedge could be unique across the transition from the Southern Apennines to the Calabrian Arc. This hypothesis is also supported by the direction of symmetry between different station, which show a simple pattern, i.e. trench normal. This pattern is usually related, in subduction zones, to the mantle flow that follows a slowly retreating slab. In such case, the mantle wedge directly in front of the retreating slab should display a trench normal direction (Long and Silver, 2008). Local studies of anisotropy direction based SKS waves did give different results, where SKS splitting measurements furnish an almost trench parallel direction and seem to indicate the direction of flow at depth, behind the slab (i.e. escaping from behind a retreating slab, Margheriti et al., 2014).

Conversely, the second, deeper, anisotropic layer considered in our parameterization, which, following Piana Agostinetti et al. (2008b), represents the subducted crust, displays relevant differences between the stations deployed to the North at the tip of the Southern Apennines, with respect to the stations to the South. Due to the difficulties in retrieving the "polarity" of the aisotropy in this layer (positive or negative) we do not have clues to define the mechanism which produce such anisotropic behavior. Nevertheless, we can extract relevant information about the subducted crust from our results. In the North, the anisotropic layer is generally about 20 km think, its anisotropic magnitude is higher and it is located deeper with respect to the stations in the South. These indications suggest the presence of a thick slice of continental crust still on top of the slab, undergoing metamorphism leading to blueschist facies, consistent with laboratory measurements and theoretical computations (Fujimoto et al., 2007; van Keken et al., 2011; Kim et al., 2013) and with what already found in the Northern

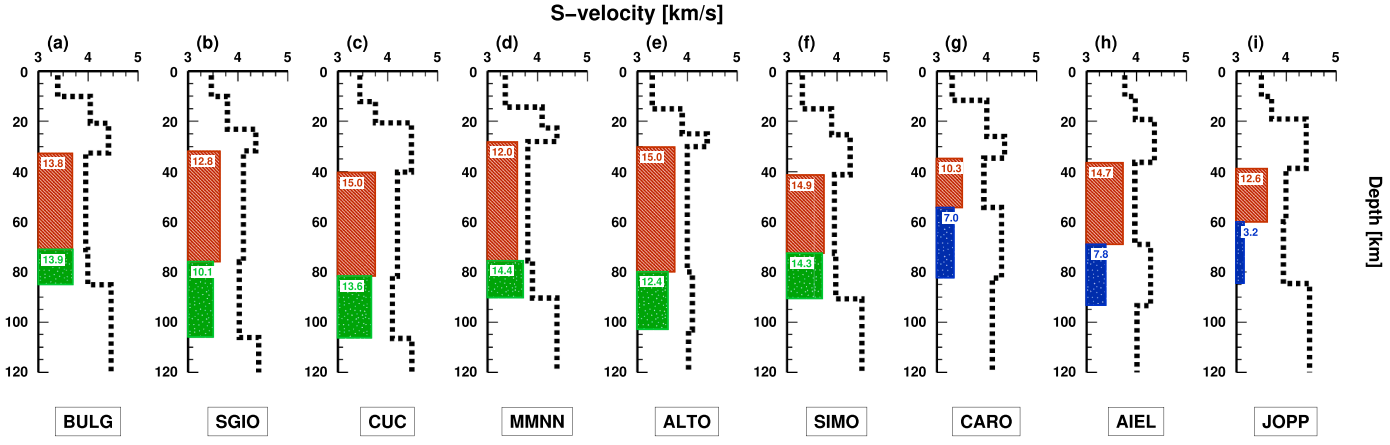

Fig. 5. Results of the inversion of the RF data-set, using a neighbourhod algorithm, in terms of best-fit models. The 1D isotropic S-wave velocity, together with the anisotropic intensity for the mantle wedge stratification, are reported for each station. Green and blue rectangles indicate (hyphotised) continental and oceanic subducted crust, respectively.

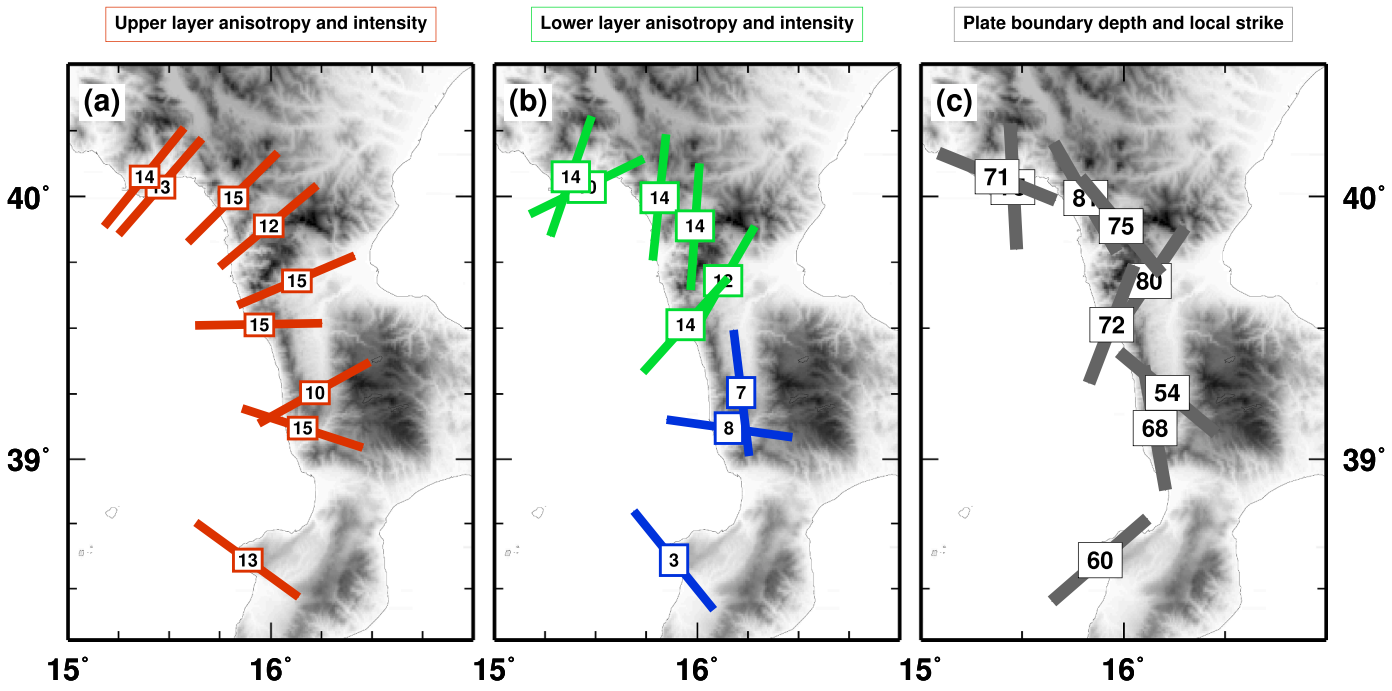

Fig. 6. Results of the inversion of the RF data-set, using a neighbourhod algorithm, in terms of best-fit models. (a) Azimuthal direction of the anisotropic axis in the upper anisotropic layer (red oriented bars), with the reported anisotropic intensity (red numbers). (b) Azimuthal direction of the anisotropic axis in the lower anisotropic layer (colored oriented bars), with the reported anisotropic intensity. Blue (Green) bars refer to hypothesized subduction of oceanic (continental) materials. (c) Depth and strike of the hypothesized plate boundary.

Apennines (Piana Agostinetti et al., 2011). Moreover, the S-wave velocity jump at its base could represent the subducted Moho, as seen in Piana Agostinetti and Miller (2014). In the South, the same anisotropic layer has a lower magnitude and it generally occurs shallower. The S-wave velocity jump at the top of such layer could indicate that the subducted crust is still not going into its metamorphic process (or starting the process leading to greenschist facies, given the small anisotropic magnitude), thus representing the "sealed" top of the subducted oceanic slab (Audet et al., 2009). However, our interpretation is debatable because its thickness is quite large (about 20 km, as in the North) for being representative of the oceanic crust-type. Differences between the Northern and the Southern stations could be given by the differences in metamorphic stage of the subducted materials. Finally, the coherence of the direction of symmetry in the anisotropic layers, in the North, which is lacking to the South, can implies different mechanisms of deformation within the subducted crust.

The geometry of the plate boundary, represented by the interface between the two anisotropic layers in our parameterization, is aligned with the curvature of the subduction arc. However, to the North, it seems to be slightly deeper with respect to the South. The variation could occur as a step or a gentle ramp but, in any case, can indicate a potential weak zone where an incipient slab tear could be in continuity with previously mapped subvertical lithospheric discontinuity in the area (Chiarabba et al., 2016). However, our results indicate that the slab is still continuous at least at shallow depths (< 100 km), supporting the hypothesis of a local slab window as seen by a localized lack of intermediate-depth and deep seismicity, only deeper than 100 km (Chiarabba et al., 2008).

5. Conclusions

We analyze teleseismic data recorded by nine seismic stations deployed across the transition between the Southern Apennines and the Calabrian Arc, an area of active subduction in the Central Mediterranean sea. Our results shed light into the mantle wedge elastic structure in terms of both S-wave seismic velocity at depth and anisotropic behavior of the rocks material composing the mantle wedge and the subducted crust. In particular, we find that: .

1. RF analysis can be used to make punctual estimations of anisotropy in the mantle wedge, without mixing contribution from different elements of the subduction system. Anisotropy in the mantle wedge seems to be generated by alignment of the olivine crystals with the flow direction consistent by slab retreat.
2. The seismic properties of the subducted crust changes along the subduction zone, indicating a possible change in subducted crustal materials, from continental to oceanic. However, such changes could be also given by a different metamorphism of the subducted materials.
3. The geometry of the plate boundary almost follows the geometry of the trench, indicating an almost continuous subduction zone (i.e. potential slab tears should be deeper than 100 km depth);
4. The depth of the subducted crust changes from North to South, indicating that local topography of the plate boundary exists.

Our results clearly highlight differences in the subducted materials but not in the mantle wedge sensu stricto. Such differences could be linked to discontinuities in the subducted lithosphere. In the future, data from temporary experiments in the area could furnish additional finer details on the slab topography closer to the transition.

CRediT authorship contribution statement

Nicola Piana Agostinetti: Conceptualization, Data curation, Formal analysis, Investigation, Methodology, Visualization, Writing – original draft, Writing – review & editing.

Declaration of Competing Interest

The authors declare that they have no known competing financial interests or personal relationships that could have appeared to influence the work reported in this paper.

Data availability

Data are already available on publi repositories (EIDA/IRIS).

Acknowledgments

NPA thanks Andrew Frederiksen and Malcolm Sambridge for providing RAYSUM and NA codes, respectively. All the computations have been done on INGV cluster. NPA is deeply in debt with Daniele Melini for support in using the INGV cluster infrastructure. Figures are drawn using GMT software (Wessel and Smith, 1998). Seismic data can be retrieved from EIDA (https://www.orfeus-eu.org/data/eida/) and IRIS (https://www.iris.edu/hq/sis/data/) data centers. The complete ensemble of elastic models used to compute Figures 5 and Figures 6 can be found in the open-access repository: Bicocca Open Archive Research Data (https://board.unimib.it/research-data/).

References

Abers, G., MacKenzie, L.S., Rondenay, S., Zhang, Z., Wech, A.G., Creager, K.C., 2009. Imaging the source region of Cascadia tremor and intermediate-depth earthquakes. Geology 37, 1119–1122. https://doi.org/10.1130/G30143A.1.

Amato, A., Bianchi, I., Piana Agostinetti, N., 2014. Apulian crust: top to bottom. J. Geodyn. 82, 125–137. https://doi.org/10.1016/j.jog.2014.09.007 ({SI}: Geodynamics of the Mediterranean).

Audet, P., 2015. Layered crustal anisotropy around the San Andreas Fault near Parkfield, California. J. Geophys. Res. Solid Earth 120, 3527–3543. https://doi.org/10.1002/2014JB011821.

Audet, P., Bostock, M.G., Christensen, N.I., Peacock, S.M., 2009. Seismic evidence for overpressured subducted oceanic crust and megathrust fault sealing. Nature 457, 76–78. https://doi.org/10.1038/nature07650.

Bianchi, I., Chiarabba, C., Piana Agostinetti, N., 2010a. Control of the 2009 L'Aquila earthquake, central Italy, by a high velocity structure: a receiver function study. J. Geophys. Res. 115. https://doi.org/10.1029/2009JB007087.

Bianchi, I., Park, J., Piana Agostinetti, N., Levin, V., 2010b. Mapping seismic anisotropy using harmonic decomposition of receiver functions: an application to Northern Apennines, Italy. J. Geophys. Res 115, B12317. https://doi.org/10.1029/2009JB007061.

Bianchi, I., Piana Agostinetti, N., De Gori, P., Chiarabba, C., 2008. Deep structure of the Colli Albani volcanic district (central Italy) from receiver functions analysis. J. Geophys. Res. 113, B09313 https://doi.org/10.1029/2007JB005548.

Blackman, D.K., Kendall, J.M., 2002. Seismic anisotropy in the upper mantle 2. predictions for current plate boundary flow models. Geochem. Geophys. Geosyst. 4. https://doi.org/10.1029/2001GC000247.

Buttles, J., Olson, P., 1988. A laboratory model of subduction zone anisotropy. Earth Planet. Sci. Lett. 164, 245–262.

Caló, M., Dorbath, C., Luzio, D., Rotolo, S., D'Anna, G., 2012. Seismic velocity structures of southern Italy from tomographic imaging of the Ionian slab and petrological inferences. Geophys. J. Int. 191, 751–764.

Chiarabba, C., Agostinetti, N.P., Bianchi, I., 2016. Lithospheric fault and kinematic decoupling of the apennines system across the pollino range. Geophys. Res. Lett. 43, 3201–3207. https://doi.org/10.1002/2015GL067610.

Chiarabba, C., De Gori, P., Speranza, F., 2008. The southern Tyrrhenian subduction zone: deep geometry, magmatism and Plio-Pleistocene evolution. Earth Planet. Sci. Lett. 268, 408–423.

Chiarabba, C., Jovane, L., DiStefano, R., 2005. A new view of italian seismicity using 20 years of instrumental recordings. Tectonophysics 395, 251–268.

Cioni, R., 2000. Volatile content and degassing processes in the AD 79 magma chamber at Vesuvius (Italy). Contrib. Mineral. Pet. 140, 40–54.

Civello, S., Margheriti, L., 2004. Toroidal mantle flow around the calabrian slab (italy) from sks splitting. Geophys. Res. Lett. 31. https://doi.org/10.1029/2004GL019607.

Di Bona, M., 1998. Variance estimate in frequency–domain deconvolution for teleseismic receiver function computation. Geophys. J. Int. 134, 634–646.

Di Bona, M., Lucente, F.P., Piana Agostinetti, N., 2008. Crustal structure and Moho depth profile crossing the central Apennines (Italy) along the N° 42 parallel. J. Geophys. Res. 113. https://doi.org/10.1029/2008JB005625.

Díaz, J., Gil, A., Gallart, J., 2012. Uppermost mantle seismic velocity and anisotropy in the Euro-Mediterranean region from Pn and Sn tomography. Geophys. J. Int. 192, 310–325. https://doi.org/10.1093/gji/ggs016.

Engdahl, E., Villaseñor, A., 2002. 41 - global seismicity: 1900-1999. In: Lee, W.H., Kanamori, H., Jennings, P.C., Kisslinger, C. (Eds.), International Handbook of Earthquake and Engineering Seismology, Part A. Academic Press. volume 81 of International Geophysics, 192, pp. 665–cp2. https://doi.org/10.1016/S0074-6142(02)80244-3.

Faccenda, M., Capitanio, F.A., 2013. Seismic anisotropy around subduction zones: Insights from three-dimensional modeling of upper mantle deformation and SKS splitting calculations. Geochem. Geophys. Geosys. 14, 243–262. https://doi.org/10.1002/ggge.20055.

Faccenna, C., Becker, T.W., Lucente, F.P., Jolivet, L., Rossetti, F., 2001. History of subduction and back-arc extension in the Central Mediterranean. Geoph. J. Int. 145, 809–820.

Farra, V., Vinnik, L., 2000. Upper mantle stratification by P and S receiver functions. Geophys. J. Int. 141, 699–712.

Fichtner, A., Bowden, D., Ermert, L., 2020. Optimal processing for seismic noise correlations. Geophys. J. Int. 223, 1548–1564. https://doi.org/10.1093/gji/ggaa390.

Frederiksen, A.W., Bostock, M.G., 2000. Modeling teleseismic waves in dipping anisotropic structures. Geophys. J. Int. 141, 401–412.

Fujimoto, Y., Kono, Y., Ishikawa, M., Hirajima, T., Arima, M., 2007.Vp and Vs Measurements of Blueschists: Implications for the Origin of High-poisson s Ratio Anomalies in the Subducting Slab.Japan Geoscience Union.

Giacomuzzi, G., Civalleri, M., De Gori, P., Chiarabba, C., 2012. A 3D Vs model of the upper mantle beneath Italy: insight on the geodynamics of central Mediterranean. Earth Pla. Sci. Lett. 335–336, 105–120.

Giacomuzzi, G., De Gori, P., Chiarabba, C., 2022. How mantle heterogeneities drive continental subduction and magmatism in the apennines. Sci. Rep. 12, 13631.

Girardin, N., Farra, V., 1998. Azimuthal anisotropy in the upper mantle from observation of P-to-S converted phases: application to southeast Australia. Geophys. J. Int. 133, 615–629.

Hacker, B.R., Abers, G., Peacock, S., 2003. Subduction factory 1. Theoretical mineralogy, densities, seismic wave speeds, and H_2 O contents. J. Geophys. Res. 108. https://doi.org/10.1029/2001JB001127.

Heuret, A., Lallemand, S., Funiciello, F., Piromallo, C., Faccenna, C., 2011. Physical characteristics of subduction interface type seismogenic zones revisited. Geochem. Geophys. Geosys. 12. https://doi.org/10.1029/2010GC003230.

Kenyon, L.M., Wada, I., 2022. Shear-wave splitting in the mantle wedge: role of elastic tensor symmetry of olivine aggregates. Geophys. Res. Lett. n/a, e2022GL100143 https://doi.org/10.1029/2022GL100143.

Kim, D., Katayama, I., Michibayashi, K., Tsujimori, T., 2013. Deformation fabrics of natural blueschists and implications for seismic anisotropy in subducting oceanic crust. Phys. Earth Planet. Inter. 222, 8–21.

Lamarque, G., Piana Agostinetti, N., 2020. Modeling of anisotropy in the lithosphere and asthenosphere for real earth cases: a critical assessment of the impact on sks measurements. J. Geophys. Res. Solid Earth 125, e2019JB018978. https://doi.org/10.1029/2019JB018978.

Levin, V., Okaya, D., Park, J., 2007. Shear wave birefringence in wedge-shaped anisotropic regions. Geophys. J. Int. 168, 275–286. https://doi.org/10.1111/j.1365-246X.2006.03224.x.

Levin, V., Park, J., 1998. P-SH conversions in layered media with hexagonally symmetric anisotropy: a cookbook. Pure Appl. Geophys. 151, 669–697.

Licciardi, A., Eken, T., Taymaz, T., Piana Agostinetti, N., Yolsal-Çevikbilen, S., 2018. Seismic anisotropy in central north anatolian fault zone and its implications on crustal deformation. Phys. Earth Planet. Inter. 277, 99–112. https://doi.org/10.1016/j.pepi.2018.01.012.

Long, M.D., Silver, P.G., 2008. The subduction zone flow field from seismic anisotropy: a global view. Science 319, 315–318.

Lucente, F.P., Chiarabba, C., Cimini, G.B., Giardini, D., 1999. Tomographic constraints on the geodynamic evolution of the italian region. J. Geophys. Res. 104, 20307–20327.

Margheriti, L., Lucente, F., Park, J., Pondrelli, S., Levin, V., Steckler, M., Baccheschi, P., Salimbeni, S., 2014. Large-scale coherent anisotropy of upper mantle beneath the italian peninsula comparing quasi-love waves and sks splitting. J. Geodyn. 82, 26–38. https://doi.org/10.1016/j.jog.2014.07.007.

McCrory, P.A., Blair, J.L., Waldhauser, F., Oppenheimer, D.H., 2012. Juan de Fuca slab geometry and its relation to Wadati-Benioff zone seismicity. J. Geophys. Res. 117. https://doi.org/10.1029/2012JB009407.

Nikulin, A., Levin, V., Park, J., 2009. Receiver function study of the Cascadia megathrust: evidence for localized serpentinization. Geochem. Geophys. Geosys. 10, Q07004 https://doi.org/10.1029/2009GC002376.

Park, J., Levin, V., 2016. Anisotropic shear zones revealed by backazimuthal harmonics of teleseismic receiver functions. Geophys. J. Int. 207, 1216–1243. https://doi.org/10.1093/gji/ggw323.

Piana Agostinetti, N., Bianchi, I., Amato, A., Chiarabba, C., 2011. Fluid migration in continental subduction: the Northern Apennines case study. Earth Pla. Sci. Lett. 302. https://doi.org/10.1016/j.epsl.2010.10.039.

Piana Agostinetti, N., Buttinelli, M., Chiarabba, C., 2022. Deep structure of the crust in the area of the 2016-2017 central italy seismic sequence from receiver function analysis. Tectonophysics 826, 229237. https://doi.org/10.1016/j.tecto.2022.229237.

Piana Agostinetti, N., Levin, V., Park, J., 2008a. Crustal structure above a retreating trench: receiver function study of the northern Apennines orogen. Earth Planet. Sci. Lett. 275, 211–220. https://doi.org/10.1016/j.epsl.2008.06.022.

Piana Agostinetti, N., Licciardi, A., Piccinini, D., Mazzarini, F., Musumeci, G., Saccorotti, G., Chiarabba, C., 2017. Discovering geothermal supercritical fluids: a new frontier for seismic exploration. Sci. Rep. 7. https://doi.org/10.1038/s41598-017-15118-w.

Piana Agostinetti, N., Malinverno, A., 2018. Assessing uncertainties in high-resolution, multi-frequency receiver function inversion: a comparison with borehole data. Geophysics 83, KS11–KS22. https://doi.org/10.1190/geo2017-0350.1.

Piana Agostinetti, N., Miller, M.S., 2014. The fate of the downgoing oceanic plate: insight from the Northern Cascadia subduction zone. Earth Planet. Sci. Lett. 408, 237–251. https://doi.org/10.1016/j.epsl.2014.10.016.

Piana Agostinetti, N., Park, J.J., Lucente, F.P., 2008b. Mantle wedge anisotropy in Southern Tyrrhenian subduction zone (Italy), from receiver function analysis. Tectonophysics 462, 35–48. https://doi.org/10.1016/j.tecto.2008.03.020.

Plescia, S.M., Hayes, G.P., 2020. Geometric controls on megathrust earthquakes. Geophys. J. Int. 222, 1270–1282. https://doi.org/10.1093/gji/ggaa254.

Plomerova, J., Margheriti, L., Park, J., Babuska, V., Pondrelli, S., Vecsey, L., Piccinini, D., Levin, V., Baccheschi, P., Salimbeni, S., 2006. Seismic anisotropy beneath the Northern Apennines (Italy): mantle flow or lithosphere fabric? Earth Planet. Sci. Lett. 247, 157–170.

Rondenay, S., Abers, G.A., van Keken, P.E., 2008. Seismic imaging of subduction zone metamorphism. Geology 36, 275–278. https://doi.org/10.1130/G24112A.1.

Rossi, G., Abers, G.A., Rondenay, S., Christensen, D.H., 2006. Unusual mantle poisson's ratio, subduction, and crustal structure in central Alaska. J. Geophys. Res. 111. https://doi.org/10.1029/2005JB003956.

Salimbeni, S., Pondrelli, S., Margheriti, L., Levin, V., Park, J., Plomerova, J., Babuska, V., 2007. Abrupt change in mantle fabric across Northern Apennines detected using seismic anisotropy. Geophys. Res. Lett. 34. https://doi.org/10.1029/2007GL029302.

Sambridge, M., 1999. Geophysical inversion with a neighbourhood algorithm –I. Searching a parameter space. Geophys. J. Int. 138, 479–494.

Schellart, W., Rawlinson, N., 2013. Global correlations between maximum magnitudes of subduction zone interface thrust earthquakes and physical parameters of subduction zones. Phys. Earth Planet. Inter. 225, 41–67. https://doi.org/10.1016/j.pepi.2013.10.001.

Sherrington, H.F., Zandt, G., Frederiksen, A., 2004. Crustal fabric in the Tibetan Plateau based on waveform inversion for seismic anisotropy parameters. J. Geophys. Res. 109. https://doi.org/10.1029/2002JB002345.

Shiomi, K., Park, J., 2008. Structural features of the subducting slab beneath the Kii Peninsula, central Japan: seismic evidence of slab segmentation, dehydration, and anisotropy. J. Geophys. Res. 113. https://doi.org/10.1029/2007JB005535.

Speranza, F., Minelli, L., Pignatelli, A., Chiappini, M., 2012. The ionian sea: the oldest in situ ocean fragment of the world? J. Geophys. Res. Solid Earth 117. https://doi.org/10.1029/2012JB009475.

van Keken, P.E., Hacker, B.R., Syracuse, E.M., Abers, G.A., 2011. Subduction factory 4: depth-dependent flux of H2O from subducting slabs worldwide. J. Geophys. Res. 116, B01401 https://doi.org/10.1029/2010JB007922.

Wessel, P., Smith, W.H.F., 1998. New, improved version of the generic mapping tools released. In: EOS Trans., 79. AGU, p. 579.

Wirth, E.A., Long, M.D., 2012. Multiple layers of seismic anisotropy and a low-velocity region in the mantle wedge beneath japan: evidence from teleseismic receiver functions. Geochem. Geophys. Geosys. 13. https://doi.org/10.1029/2012GC004180.